

3D Plate-Lattices: An Emerging Class of Low-Density Metamaterial Exhibiting Optimal Isotropic Stiffness

Thomas Tancogne-Dejean, Marianna Diamantopoulou, Maysam B. Gorji, Colin Bonatti, and Dirk Mohr*

In lightweight engineering, there is a constant quest for low-density materials featuring high mass-specific stiffness and strength. Additively-manufactured metamaterials are particularly promising candidates as the controlled introduction of porosity allows for tailoring their density while activating strengthening size-effects at the nano- and microstructural level. Here, plate-lattices are conceived by placing plates along the closest-packed planes of crystal structures. Based on theoretical analysis, a general design map is developed for elastically isotropic plate-lattices of cubic symmetry. In addition to validating the design map, detailed computational analysis reveals that there even exist plate-lattice compositions that provide nearly isotropic yield strength together with elastic isotropy. The most striking feature of plate-lattices is that their stiffness and yield strength are within a few percent of the theoretical limits for isotropic porous solids. This implies that the stiffness of isotropic plate-lattices is up to three times higher than that of the stiffest truss-lattices of equal mass. This stiffness advantage is also confirmed by experiments on truss- and plate-lattice specimens fabricated through direct laser writing. Due to their porous internal structure, the potential impact of the new metamaterials reported here goes beyond lightweight engineering, including applications for heat-exchange, thermal insulation, acoustics, and biomedical engineering.

The stress–strain curve reveals the stiffness and the strength of a material. It is obtained from mechanical experiments in which a block or coupon of material is subjected to uniaxial tension (or compression). The stress–strain response often depends on the orientation of the material with respect to the direction of loading. Wood, for instance, is much stiffer and stronger when loaded along its fiber direction as opposed to its radial direction.^[1] In the case of mechanical metamaterials such


as foams, honeycombs and truss-lattices, it is less obvious to recognize the loading direction sensitivity of their mechanical response. For example, a simple-cubic truss with a unit cell composed of three orthogonal beams features the same stiffness along all [100] directions, yet it is a highly anisotropic material: its stiffness along the diagonal [111] directions is several orders of magnitude lower.^[2]

At low levels of microstructural hierarchy, anisotropy can be leveraged to achieve high strength in combination with high damage tolerance.^[3,4] However, at the macroscopic level, engineering materials for large volume markets are expected to exhibit isotropic stiffness and strength. For example, all polycrystalline metals, polymers and ceramics fall into the class of nearly isotropic solids. Stochastic solid foams are the first generation of man-made porous isotropic metamaterials. These are primarily used for elastic cushioning (shape recovery) and impact energy absorption purposes.^[1] Foams achieve the direction-independent stress–strain

response through a random structure of open or closed cells. When it comes to stiffness and strength, truss-lattice materials outperform random foams for the same constituent material and the same relative density.^[1,5] Anisotropic truss-lattices received significant attention,^[6–15] before the discovery of isotropic configurations.^[16–18] Computational and experimental studies led to a mature level of understanding of the mechanical property space of 3D lattice architectures.^[18–20] Advanced material processing techniques have enabled the fabrication of truss-lattices at the micro- and nanoscales, thereby increasing their mechanical performance through tailoring the relevant length scales.^[10–12,21] Despite their superiority in stiffness to stochastic foams,^[16] the structural efficiency of the stiffest elastically isotropic truss-lattices is still not optimal. For example, at low relative densities, their stiffness attains less than 33% of the Hashin–Shtrikman (HS) bound, which is the highest theoretically achievable elastic modulus for an isotropic porous solid.^[22] Lattices composed of shells^[23] (“shellular”) and plates appear to be more promising. Using numerical analysis, Berger et al.^[24] identified one particular cubic-octet foam, which is a first example of an isotropic plate-lattice structure achieving maximum theoretical stiffness.

T. Tancogne-Dejean, M. Diamantopoulou, Dr. M. B. Gorji, C. Bonatti, Prof. D. Mohr
Department of Mechanical and Process Engineering
Swiss Federal Institute of Technology (ETH)
Tannenstrasse 3, Zurich 8006, Switzerland
E-mail: dmohr@ethz.ch

T. Tancogne-Dejean, Dr. M. B. Gorji, C. Bonatti
Department of Mechanical Engineering
Massachusetts Institute of Technology (MIT)
77 Massachusetts Avenue, Cambridge, MA 02139, USA

 The ORCID identification number(s) for the author(s) of this article can be found under <https://doi.org/10.1002/adma.201803334>.

DOI: 10.1002/adma.201803334

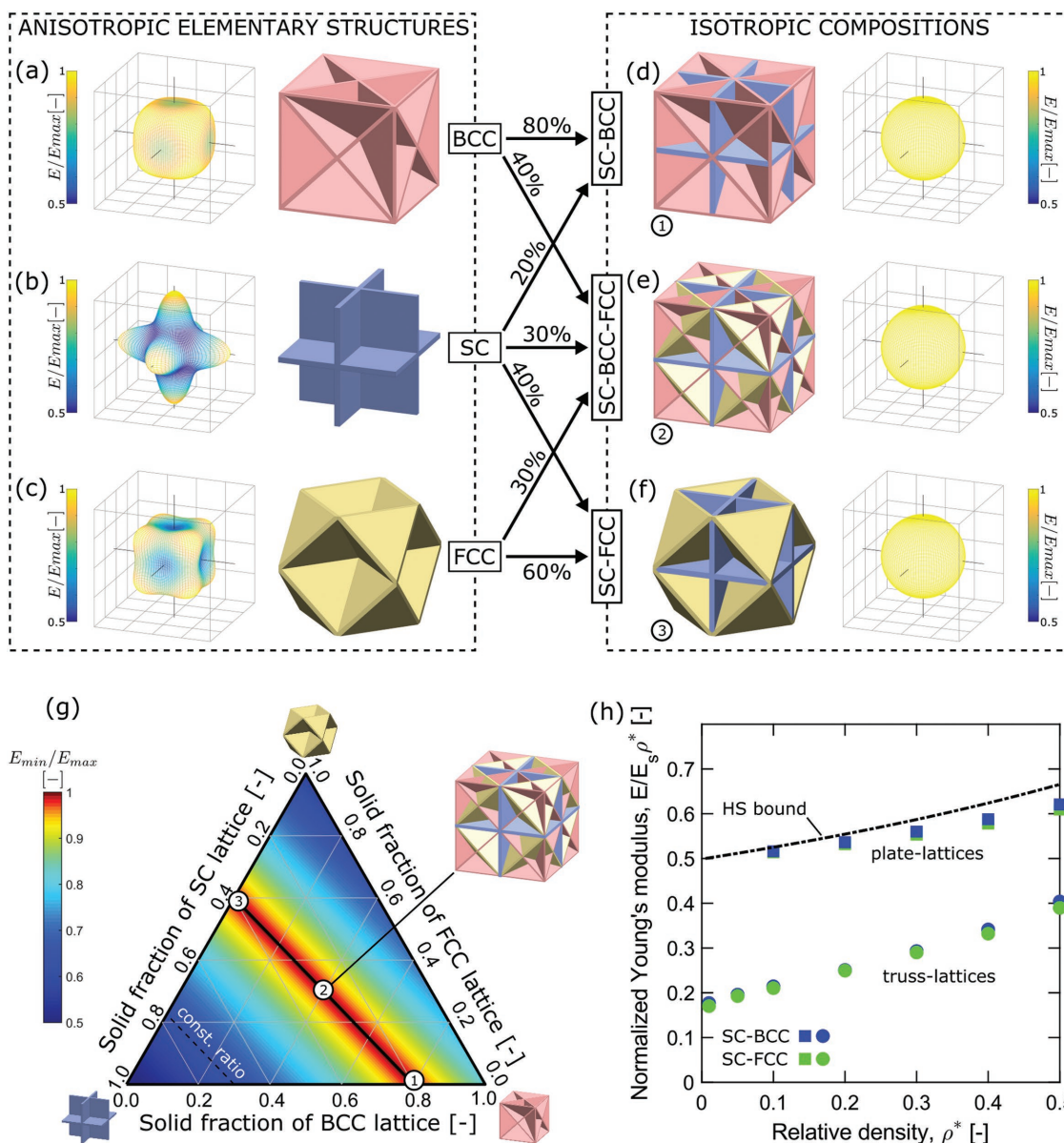


Figure 1. Stiffness of plate-lattices. a–c) Anisotropic elementary structures and their normalized uniaxial stiffness as a function of the direction of loading. The edges of the gray coordinate grids are aligned with the [100] directions of the cubic unit cells. d–f) Isotropic plate-lattice compositions obtained by mixing the elementary structures. g) Design map providing the minimum-to-maximum modulus ratio as a function of the mixing ratios of the elementary structures. The black line inside the red zone highlights all isotropic compositions. h) Scaling of normalized Young's modulus of isotropic metamaterials as a function of their relative density. Simulation results for selected isotropic plate-lattices (square dots) and truss-lattices (circular dots) are shown next to the theoretical upper limit (Hashin–Shtrikman bound).

Here, we identify a full family of elastically isotropic plate-lattices that provide near-optimal mass-specific stiffness. Moreover, we reveal novel architectures that provide not only high isotropic stiffness, but which exhibit also a nearly isotropic plastic response. Plate-lattices are fabricated using 3D direct laser writing to demonstrate experimentally their stiffness advantage over isotropic trusses of the same mass. Attention is limited to structures of cubic symmetry. Simple cubic (SC), body-centered-cubic (BCC), and face-centered-cubic (FCC) elementary plate-lattices (Figure 1a–c) are obtained by placing plates on the closest-packed planes of cubic crystals. Isotropic

plate lattices (Figure 1d–f) are then synthesized through mixing of elementary cubic structures.

Using theoretical homogenization (Supporting Information), an analytical expression for the full stiffness tensor of plate-lattices is obtained as a function of the relative density, $\rho^* = V_s/V$, i.e., the ratio of the volume V_s of the solid constituent material comprised in a unit cell of volume V . For the elementary SC, FCC, and BCC plate-lattices (Figure 1a–c), the ratios of the moduli for the softest and stiffest directions are 0.49, 0.58, and 0.83, respectively. We exploit the fact that the stiffest direction of the SC elementary structure coincides with the softest direction

of the FCC and BCC elementary structures, and vice versa. It is actually possible to combine different elementary structures in a way that the resulting compositions exhibit an elastically-isotropic response (e.g., Figure 1d–f).

The design map shown in Figure 1g provides the required solid volume fractions of the elementary cubic structures for synthesizing elastically isotropic plate-lattices. The color contour is the ratio of the minimum-to-maximum modulus, E_{\min}/E_{\max} . An infinite number of isotropic SC-BCC-FCC compositions are found (black line in the red region in Figure 1g). The limiting cases are a particular SC-BCC composition (structure ①) and the cubic-octet foam structure of Berger et al.^[24] (which corresponds to the particular SC-FCC composition ③). According to our theoretical solution at the low relative density limit, we have $\frac{E}{\rho^* E_s} \approx 0.5$ for the isotropic plate-lattices (with E and E_s denoting the Young's moduli of the lattice structure and the solid constituent material, respectively). When comparing this result with the known solution for truss-lattices,^[16,18] $\frac{E}{\rho^* E_s} = 0.17$, it becomes apparent that the identified plate-lattices are up to three times stiffer than optimal trusses of the same relative density. It is strikingly clear that, even if they respond in the ideal stretching-dominated manner, isotropic truss-lattices cannot compete with plate-lattices of equal density. Since the analytical estimates are only exact in the limit of infinitesimal relative density ($\rho^* \rightarrow 0$), we build detailed finite element models of selected plate-lattices (Experimental Section) to confirm that the elastic moduli of plate-lattices reach the Hashin–Shtrikman bound for relative densities of up to 50% (Figure 1h).

Plate-lattices are designed such that all constituent plates respond primarily through membrane deformation, as opposed to compliant-mechanism metamaterials, whose macroscopic response is governed by the bending of the constituent plates.^[25] The remarkable stiffness advantage of plate- over truss-lattices can be understood without going into the mathematical details.

Consider a first SC unit cell made from three beams of equal length L and cross-sectional area A , and a second made from three plates of area $L \times L$ and of thickness $t = A/L$ (equal volume). When these structures are subjected to uniaxial compression along the [100] direction, one of the three beams is uniformly compressed in the truss-lattice, while two of the three plates are uniformly compressed in the plate-lattice (the stretched elements are highlighted in yellow in the schematics ④ and ⑤ in Figure 2). Given that the constituent beams and plates have equal volume, and that the deformed portions of the respective solid phases experience the same amount of strain (i.e., same local strain energy density), it can be concluded that for the same macroscopic strain ϵ_M , the total strain energy introduced into the plate-lattice unit-cell is twice as high as that introduced into the truss-lattice (which implies that the apparent macroscopic stiffness of the plate-lattice is then also twice as high). The fundamental advantage of plate-lattices is that each constituent plate contributes to the load carrying capacity for all direction vectors comprised in the plane of the plate. A single beam of the same volume as a plate provides also the same stiffness, but for one predefined direction only.

After introducing the strain energy density (SED) for uniform straining of the constituent material, $\psi_s = \frac{1}{2} E_s \epsilon_M^2$, we plot the normalized distribution of the local SED ψ as a function of the fraction of solid volume comprised in a unit cell (Figure 2). In the case of the SC structures, a simple step function is obtained (when neglecting the role of intersections). We have $\psi/\psi_s = 1$ for 33% of the volume of the truss-lattice, and for 66.7% of the volume of the plate-lattice (gray curves). The SED plots become more interesting when analyzing the simulation results for uniaxial compression of the isotropic compositions along their [100] direction. In an isotropic SC-BCC truss-lattice of 30% relative density (structure ⑩ in Figure 2), the SED is $\psi/\psi_s \geq 1$ in the vertical struts aligned with the direction of loading (about 11% of the solid volume). It then drops to values of about $\psi/\psi_s \approx 0.1$ for the diagonal and horizontal members

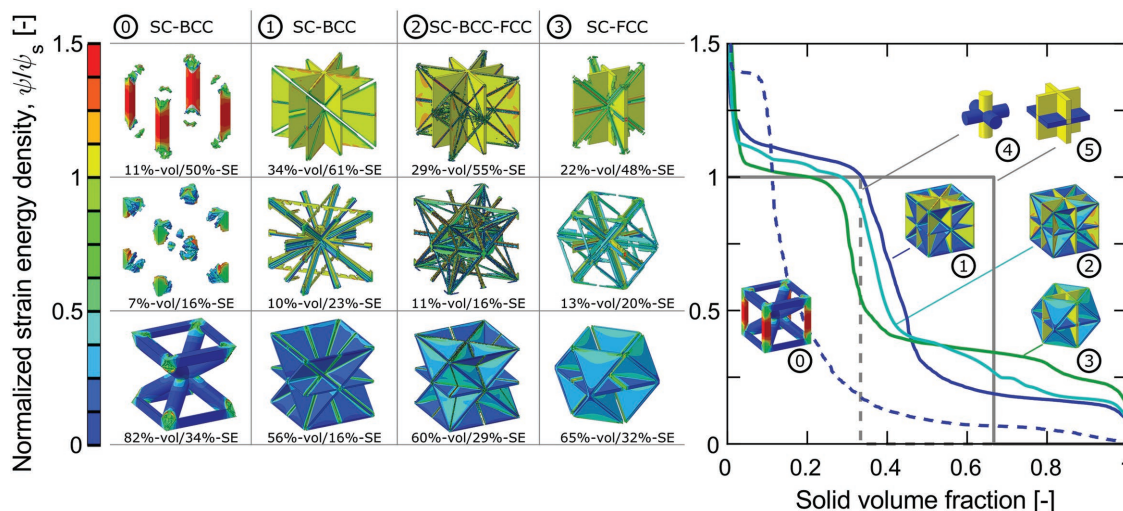


Figure 2. Distribution of the strain energy density within lattices of 30% relative density subject to uniaxial compression along the vertical direction. The contour plots and the right-hand plot show the strain energy density as normalized by the Voigt solution (uniform distribution). All insets except for the schematics ④ and ⑤ show results from finite element simulations.

(about 82% of the solid volume experiences $\psi/\psi_s < 0.5$). The integration over different parts of the truss-lattice then shows that about 50% of the total strain energy (SE) is stored in the vertical struts, even though they only make up for 11% of the volume. In case of the SC-BCC plate-lattice (structure ①), the SED is $\psi/\psi_s \geq 1$ for all vertical plates. The main difference as compared to the truss-lattice is that as much as 34% of the solid matter is comprised in these vertical plates, while only 56% is oriented along weakly strained ($\psi/\psi_s < 0.5$) diagonal and horizontal directions. As a result, the integral of the SED over the entire plate-lattice is much higher than that for the truss-lattices, which translates into a much higher stiffness at the macroscopic level. The results for other SC-BCC-FCC topologies (Figure 2) and different directions of loading (Supporting Information) lead to the same conclusions: the SED in plate-lattices is always more uniform (smaller min/max deviations from the average SED), while the solid volume fraction experiencing an SED greater than ψ_s is always at least twice as high in the plate-lattices as in the truss-lattices of equal mass.

To validate our stiffness estimates experimentally, we use 3D direct laser writing to fabricate truss- and plate-lattices with a cubic unit cell size of 66 μm from a glassy polymer (Figure 3a–l). For the SC-BCC and SC-FCC plate-lattices, a relative density of $\rho^* = 30\%$ is obtained for SC (BCC/FCC) plate thicknesses of 1.5(2.1) and 3.0(2.0) μm , respectively. For the SC-BCC and SC-FCC truss-lattices, the corresponding SC (BCC/FCC) beam

diameters are 17.4(14.0) and 12.2(10.3) μm , respectively. The main road block to date for manufacturing plate-lattices through liquid-bath or powder-bed based additive processes is that excess liquid or powder is trapped inside the closed cells formed by the plates. Here, circular holes of a diameter of 5.3 μm are placed at the center of each plate to allow for the extraction of unexposed liquid photoresist (at the expense of less than 5% of the plate-lattice stiffness, see Supporting Information).

The elastic moduli are determined through linear regression of the initial slope of the stress–strain curves measured during uniaxial compression experiments. The average moduli are 332 and 151 MPa for the plate- and truss-lattices, respectively (Figure 3m). This equates to a stiffness ratio of 2.1 which is close to the stiffness ratio of 1.9 expected from numerical simulations for $\rho^* = 30\%$. As anticipated from the numerically predicted spatial distribution of the strain energy density (Figure 2), the experimental observations for moderate strains show that the vertical plates and struts are the first to fail through buckling (Figures 3n,o). A detailed discussion and videos of the large deformation response are provided in the Supporting Information. Given the viscoplastic nature of the constituent material, the plastic yield response cannot be quantified from the experimental measurements. Instead, another series of simulations is performed to investigate the yield strength of plate-lattices using a rate-independent model for the constituent material.

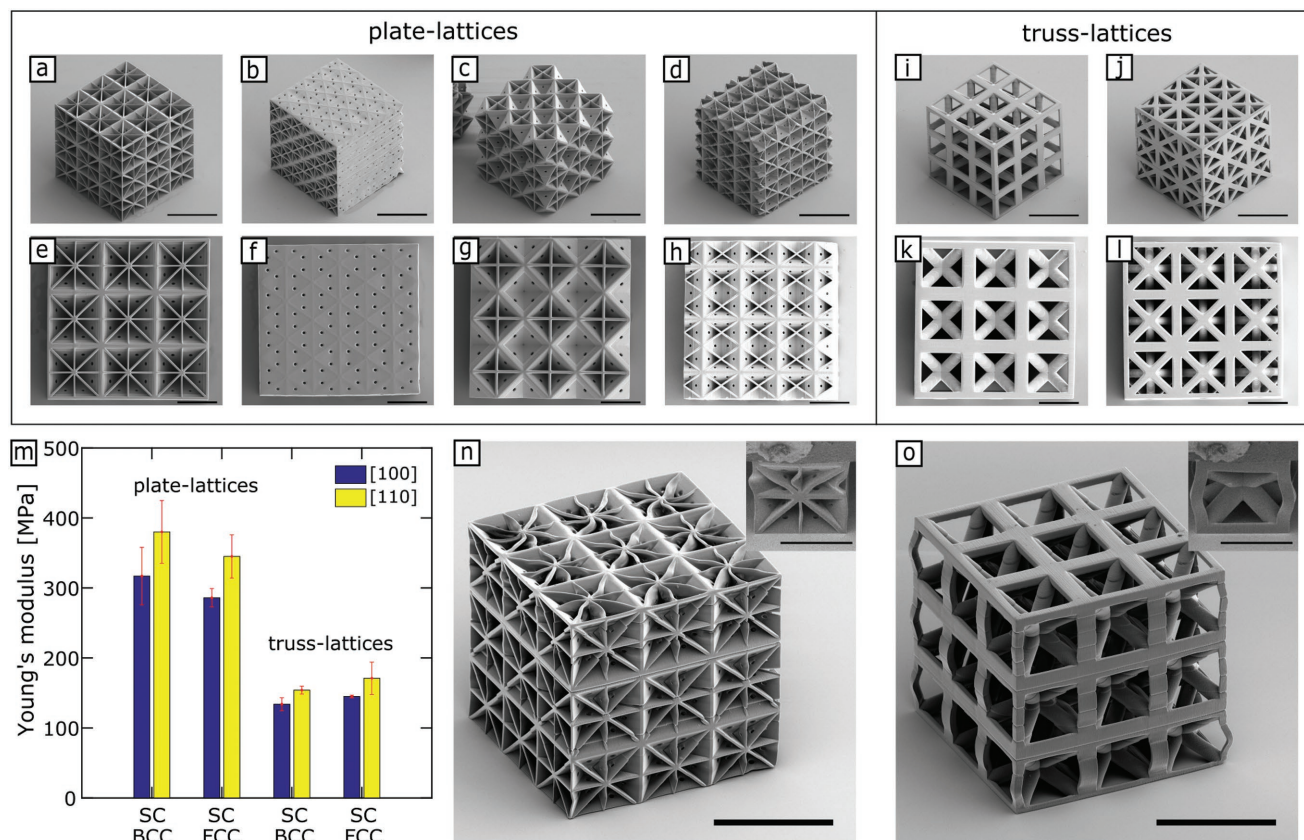


Figure 3. Polymer specimens of 30% relative density fabricated through direct laser writing. a–d) Isometric views of plate-lattice specimens: (a) [100]-SC-BCC, (b) [110]-SC-BCC, (c) [100]-SC-FCC, (d) [110]-SC-FCC. e–h) Corresponding top views. i–l) isometric and top views of [100] SC-BCC and SC-FCC truss-lattice specimens. m) Measured Young's moduli. n–o) Isometric views of deformed unit cells after applying $\approx 15\%$ compression strain along vertical direction. Scale bars: (a)–(d), (i)–(l), (n)–(o) 100 μm , (e)–(h), (k)–(l), insets in (n)–(o) 50 μm .

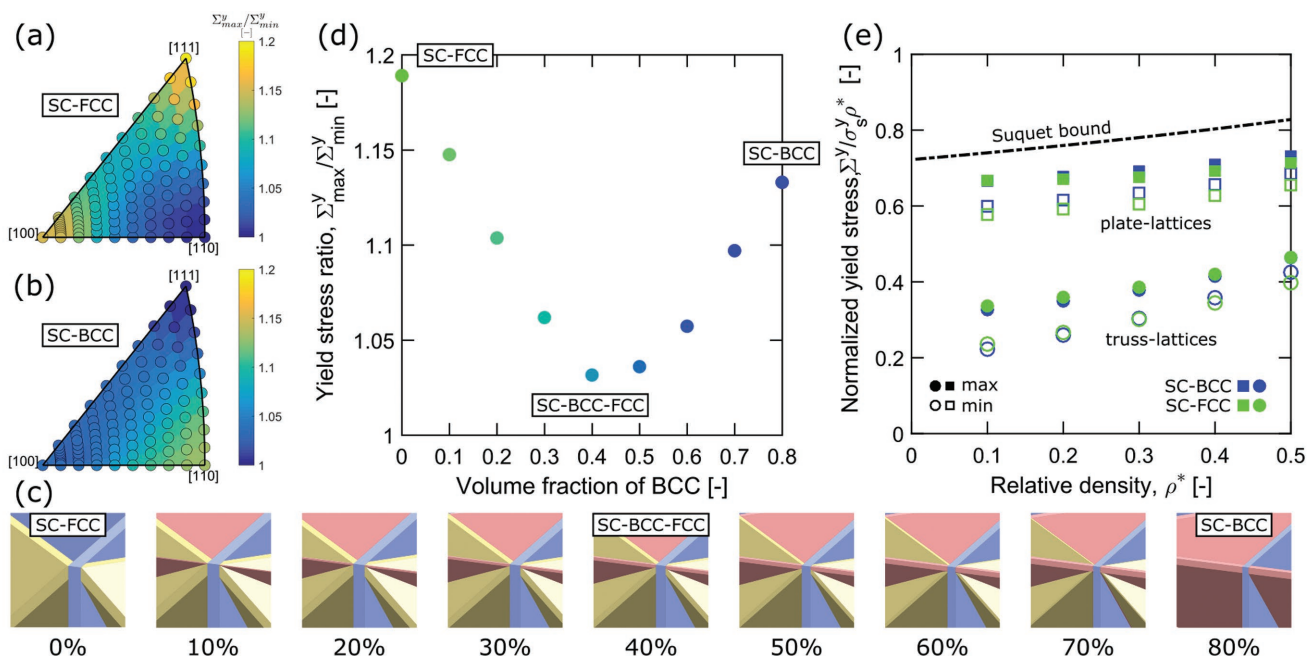


Figure 4. Yield strength of elastically isotropic metamaterials. Pole figures for the computed yield strength distribution of plate-lattices: a) SC-FCC, and b) SC-BCC. c) Detailed view of the intersection of the FCC (yellow), SC (blue), and BCC (red) elementary structures in elastically isotropic plate-lattice compositions of 20% relative density. The percentage below each view is the BCC volume fraction of the solid phase. d) Yield stress ratio as a function of the volume fraction of the BCC plates in elastically isotropic SC-BCC-FCC composition. e) Normalized yield stress as a function of the relative density. For each configuration (truss- or plate-lattice, SC-BCC or SC-FCC), the maximum (solid dot) and minimum (open dot) yield strengths are shown.

It is important to recognize that elastic isotropy does not guarantee plastic isotropy. The effective elastic response is determined by the spatial average of the local stresses over the entire volume of the unit cell. In the case of plasticity, local stress variations are decisive, i.e., if the local stresses at some material point cause the constituent material to deform plastically, the overall response of the metamaterial becomes non-linear. In a second series of simulations, the constituent solid is modeled as an isotropic elastoplastic material with isotropic strain hardening mimicking the stress–strain response of stainless steel 316L. The yield strength of the metamaterial is defined by the stress applied at the instant when the permanent deformation attains 0.2% for uniaxial loading. The pole figures (Figure 4a,b) display the orientation dependence of the yield strength of the SC-FCC and SC-BCC plate-lattices. The extreme value ratios are $\Sigma^y_{max}/\Sigma^y_{min} = 1.19$ and 1.14 for the SC-FCC and SC-BCC plate-lattices, respectively.

To identify possibly plastically isotropic configurations within the family of SC-BCC-FCC compositions, we computed the response of seven distinct elastically isotropic configurations (Figure 4c) that lie between the limiting SC-FCC and SC-BCC configurations (Figure 1g). After conducting 91 elastoplastic shell element simulations per configuration, the corresponding maximum-to-minimum yield stress ratios are plotted in Figure 4d as a function of the BCC solid volume fraction. The plot reveals a nonmonotonic relationship, with a local minimum of $\Sigma^y_{max}/\Sigma^y_{min} = 1.03 \approx 1$. In other words, within the new family of elastically isotropic plate-lattice configurations, there exists also an SC-BCC-FCC member (with a BCC solid volume fraction of about 40%), that attains not only the theoretical stiffness limit, but that is also nearly plastically isotropic! With

regards to the structural efficiency, it is noted that the yield strength of the isotropic plate-lattices (Figure 4e) of low relative density reaches about 68% of the yield strength $\rho^* \sigma^y_s$ of a hypothetical, homogeneously strained solid of equal mass. This value is very close to Suquet's (1993) yield strength bound of $0.72 \rho^* \sigma^y_s$ for isotropic porous media.^[26] The obtained (approximately) isotropic metamaterial is therefore close to being optimal from the point of view of stiffness and yield strength. This optimality also becomes apparent when comparing the plate-lattice results with the yield stress estimates for the isotropic truss-lattices (Figure 4e). Similar to the stiffness, the yield strength of plate-lattices is substantially higher than that of truss-lattices of equal mass.

In summary, using theoretical and computational mechanics, we have identified a class of metamaterial composed of plates that exhibit near-optimal isotropic stiffness. Within this family of plate-lattice compositions of cubic symmetry, we identified one particular architecture composed of SC, BCC, and FCC elementary structures which combines isotropic stiffness and (nearly) isotropic yield strength, with both properties being close to the theoretical limits for isotropic porous solids. The obtained results demonstrate that the stiffness and yield strength of plate-lattices is always higher than that of truss-lattices, with a maximum advantage in stiffness of 200% at low relative densities. In the future, the size-strengthening principle “smaller is stronger”^[9,27] also needs to be explored for plate-lattices. Unprecedented mass specific strength and recoverability are expected to be obtained by reducing the thickness of the constituent plates to nanometric dimensions (e.g., through pyrolysis^[12]) and/or by applying high entropy alloy coatings.^[21] In view of the constant progress in additive manufacturing

technology, it is likely that the newly discovered isotropic SC-BCC-FCC plate-lattices will be used in targeted applications that require materials combining low density with high specific stiffness and strength.

Experimental Section

Fabrication: Specimens of approximate dimensions $200 \times 200 \times 200 \mu\text{m}^3$ were fabricated from IP-S photoresist using two-photon polymerization direct laser writing (Photonic Professional GT, Nanoscribe GmbH) with a laser power of 50 mW and at a writing speed of 10 mm s^{-1} . All structures were fabricated in the dip-in mode on glass substrates which are cleaned prior to the fabrication with isopropyl alcohol in ultrasonic bath.

Experiments: Compression experiments were performed using a custom-made displacement-controlled microtesting device. The machine features a 5-axis stage onto which the glass substrate with the specimens was mounted. Prior to testing, the specimens were aligned with respect to a flat punch $1 \text{ mm} \times 0.5 \text{ mm}$ that was connected with a strain-gaged load cell (Omega, LCAE 6N). The loading was applied by moving the punch with a piezoelectric motor (Micromo, model LEGS Linear Twin 40N). A punch speed of $1 \mu\text{m s}^{-1}$ was prescribed in all experiments. The displacement of the punch was monitored using an optical microscope (Keyence VHX-5000) at $1000\times$ magnification with a frequency of 15 Hz. Digital image correlation (VIC-2D, Correlated Solutions) is used to measure the displacement of the punch.

Simulations: Nonlinear finite element simulations were performed using the implicit solver of the commercial software package Abaqus. All reported numerical results were based on unit cell analysis with periodic boundary conditions.^[28] Unless stated otherwise, solid element meshes were employed featuring at least five first-order solid elements along the direction of plate thickness or beam diameter. For the sake of computational efficiency, shell element meshes were used when estimating the elastoplastic response of the SC-BCC-FCC plate-lattices.

Supporting Information

Supporting Information is available from the Wiley Online Library or from the author.

Acknowledgements

This work was supported through the SNF grant 200021-165939. T.T., M.G., and C.B. acknowledge partial financial support through the MIT Industrial Fracture Consortium.

Conflict of Interest

The authors declare no conflict of interest.

Keywords

additive manufacturing, isotropy, metamaterials, stiffness, yield strength

Received: May 25, 2018

Revised: August 12, 2018

Published online:

- [1] L. J. Gibson, M. F. Ashby, *Cellular Solids*, Cambridge University Press, Cambridge, UK **1997**.
- [2] V. S. Deshpande, M. F. Ashby, N. A. Fleck, *Acta Mater.* **2001**, *49*, 1035.
- [3] F. Bouville, E. Maire, S. Meille, B. Van de Moortèle, A. J. Stevenson, S. Deville, *Nat. Mater.* **2014**, *13*, 508.
- [4] U. G. K. Wegst, H. Bai, E. Saiz, A. P. Tomsia, R. O. Ritchie, *Nat. Mater.* **2015**, *14*, 23.
- [5] J. L. Grenestedt, *Int. J. Solids Struct.* **1999**, *36*, 1471.
- [6] V. S. Deshpande, N. A. Fleck, M. F. Ashby, *J. Mech. Phys. Solids* **2001**, *49*, 1747.
- [7] L. C. Montemayor, W. H. Wong, Y.-W. Zhang, J. R. Greer, *Sci. Rep.* **2016**, *6*, 20570.
- [8] Z. He, F. Wang, Y. Zhu, H. Wu, H. S. Park, *J. Mech. Phys. Solids* **2017**, *101*, 133.
- [9] W. Gu, J. R. Greer, *Extreme Mech. Lett.* **2015**, *2*, 7.
- [10] X. Zheng, H. Lee, T. H. Weisgraber, M. Shusteff, J. DeOtte, E. B. Duoss, J. D. Kuntz, M. M. Biener, Q. Ge, J. A. Jackson, S. O. Kucheyev, N. X. Fang, C. M. Spadaccini, *Science* **2014**, *344*, 1373.
- [11] D. Jang, L. R. Meza, F. Greer, J. R. Greer, *Nat. Mater.* **2013**, *12*, 893.
- [12] J. Bauer, A. Schroer, R. Schwaiger, O. Kraft, *Nat. Mater.* **2016**, *15*, 438.
- [13] L. R. Meza, S. Das, J. R. Greer, *Science* **2014**, *345*, 1322.
- [14] T. Tancogne-Dejean, A. B. Spierings, D. Mohr, *Acta Mater.* **2016**, *116*, 14.
- [15] J. Bauer, L. R. Meza, T. A. Schaedler, R. Schwaiger, X. Zheng, L. Valdevit, *Adv. Mater.* **2017**, *29*, 1701850.
- [16] G. Gurtner, M. Durand, *Proc. R. Soc. A: Math. Phys. Eng. Sci.* **2014**, *470*, 20130611.
- [17] M. C. Messner, *J. Mech. Phys. Solids* **2016**, *96*, 162.
- [18] T. Tancogne-Dejean, D. Mohr, *Int. J. Solids Struct.* **2018**, *138*, 24.
- [19] L. R. Meza, G. P. Phlipot, C. M. Portela, A. Maggi, L. C. Montemayor, A. Cornella, D. M. Kochmann, J. R. Greer, *Acta Mater.* **2017**, *140*, 424.
- [20] C. M. Portela, J. R. Greer, D. M. Kochmann, *Extreme Mech. Lett.* **2018**, *22*, 138.
- [21] X. Zhang, J. Yao, B. Liu, J. Yan, L. Lu, Y. Li, H. Gao, X. Li, *Nano Lett.* **2018**, *18*, 4247.
- [22] Z. Hashin, S. Shtrikman, *J. Mech. Phys. Solids* **1963**, *11*, 127.
- [23] S. C. Han, J. W. Lee, K. Kang, *Adv. Mater.* **2015**, *27*, 5506.
- [24] J. B. Berger, H. N. G. Wadley, R. M. McMeeking, *Nature* **2017**, *543*, 533.
- [25] J. B. Hopkins, *Mech. Sci.* **2013**, *4*, 319.
- [26] P. M. Suquet, *J. Mech. Phys. Solids* **1993**, *41*, 981.
- [27] X. Li, H. Gao, *Nat. Mater.* **2016**, *15*, 373.
- [28] M. Danielsson, D. M. Parks, M. C. Boyce, *J. Mech. Phys. Solids* **2002**, *50*, 351.